Materials Chemistry and Physics 136 (2012) 167–172

Contents lists available at SciVerse ScienceDirect

Materials Chemistry and Physics

journal homepage: www.elsevier.com/locate/matchemphys

Synthesis and electrical characteristics of $(1-x)BaTiO_3-xK_{0.5}Bi_{0.5}TiO_3$ PTCR ceramics

T.A. Plutenko, O.I. V'yunov*, A.G. Belous

Department of Solid State Chemistry, Vernadskii Institute of General and Inorganic Chemistry, 32/34 Palladina Ave., 03142 Kyiv, Ukraine

HIGHLIGHTS

- $BaTiO_3-K_{0.5}Bi_{0.5}TiO_3$ samples were synthesized by solid state reactions technique.
- Resistance of ceramic increases with x due to a decrease in ceramic's grain size.
- With increasing x, the potential barrier at grain boundaries increases.
- Specimens of $BaTiO_3-K_{0.5}Bi_{0.5}TiO_3$ with Curie temperature up to 220 °C were obtained.
- The outer layer and the grain boundary make a contribution to the PTCR effect.

ARTICLE INFO

Article history:
Received 9 November 2011
Received in revised form
12 June 2012
Accepted 23 June 2012

Keywords:
Ceramics
Sintering
Rietveld analysis
Electrical properties

ABSTRACT

Solid solutions of $(1-x)BaTiO_3-xK_{0.5}Bi_{0.5}TiO_3$ were prepared by the solid state reaction technique. Samples were sintered in reducing atmosphere of N_2/H_2 in the temperature range 1100–1240 °C with subsequent oxidation at 700 °C. Phase composition and crystal structure were investigated by X-ray powder diffractometry (XRPD). It was shown that all samples of $(1-x)BaTiO_3-xK_{0.5}Bi_{0.5}TiO_3$ ($0 \le x < 0.4$) exhibit a tetragonal structure at room temperature, the parameters a and c decrease with increasing x. With increasing x the Curie temperature of solid solutions $(1-x)BaTiO_3-xK_{0.5}Bi_{0.5}TiO_3$ ($0.1 \le x < 0.4$) increases from 150 to 220 °C. The values of potential barriers at grain boundaries were calculated on the basis of Heywang model. With increasing x, the potential barrier at grain boundaries increases. It was shown that the grain size decreases with increasing the bismuth–potassium titanate content. The complex impedance results indicate that the grain boundary and the outer layer region, located between the boundary and the core of the grain, make a contribution to the positive temperature coefficient of resistance (PTCR) effect in $(1-x)BaTiO_3-xK_{0.5}Bi_{0.5}TiO_3$ solid solutions. With increasing x ρ_{max} increases due to an increase in potential barrier at grain boundaries.

1. Introduction

It is known that donor-doped barium titanate possesses positive temperature coefficient of resistance (PTCR) effect near the phase transition temperature (120 °C) [1]. A shift of the phase transition temperature toward low or high temperatures was achieved by partial substitution of Ba^{2+} ions by Sr^{2+} or Pb^{2+}, respectively [2,3]. However, lead-containing materials are highly toxic [4]. Therefore, it is urgent to develop lead-free PTCR materials with high Curie temperatures (above 120 °C). Substitution of potassium and bismuth ions for barium ions in $(1-x)BaTiO_3-xK_{0.5}Bi_{0.5}TiO_3$ leads to an increase in Curie temperature from 120 °C ($x = 0$) to 380 °C ($x = 1$) [5]. In addition, it was shown that in the $(1-x)BaTiO_3-xK_{0.5}Bi_{0.5}TiO_3$ system at low x ($x \le 0.1$), materials with PTCR effect can be prepared. In this case the phase transition temperature does not exceed 170 °C [6–8]. Therefore it is important to study the system $(1-x)BaTiO_3-xK_{0.5}Bi_{0.5}TiO_3$ with $x > 0.1$.

In this study, solid solutions $(1-x)BaTiO_3-xK_{0.5}Bi_{0.5}TiO_3$ were synthesized by solid state reaction technique. The effects of bismuth–potassium titanate content on the crystal structure, microstructure and electrical properties of solid solutions $(1-x)BaTiO_3-xK_{0.5}Bi_{0.5}TiO_3$ were investigated. Complex–plane impedance analysis was carried in a wide temperature range to study the electrical properties of different areas of grain and their impact on PTCR effect in solid solutions $(1-x)BaTiO_3-xK_{0.5}Bi_{0.5}TiO_3$.

2. Experimental

$(1-x)BaTiO_3-xK_{0.5}Bi_{0.5}TiO_3$ ($0 \le x \le 0.4$) solid solutions were prepared by the solid-state reaction technique. Extra-pure (purity

* Corresponding author. Tel./fax: +380 44 4242211.
E-mail address: vyunov@ionc.kiev.ua (O.I. V'yunov).

0254-0584/$ – see front matter © 2012 Elsevier B.V. All rights reserved.
http://dx.doi.org/10.1016/j.matchemphys.2012.06.047

99.99%) K_2CO_3, $BaCO_3$, Bi_2O_3 and TiO_2 (rutile) were used as initial reagents. The powders were mixed and ball-milled with ethyl alcohol in an agate mortar for 4 h. After that the mixtures were dried at 100–120 °C, passed through a nylon sieve, and then calcined in air at 950–1000 °C for 2–4 h. The resultant powders were ground with the addition of 10% polyvinyl alcohol, pressed into pellets (10 mm in diameter and 2 mm in thickness) by uniaxial pressing at 150 MPa. Pellets (85–94% theoretical density) were sintered in a flow of a gas mixture N_2/H_2 (99.5:0.5) in the temperature range 1100–1240 °C with subsequent oxidation at 700 °C. The aluminum electrodes were deposited onto the surfaces of specimens by firing of aluminum paste PA-6101 (Scientific-Research Technological Institute of Instrument, Kharkov, Ukraine). The heating and cooling rates for all samples were 300 °C h^{-1}.

The phases were characterized by X-ray powder diffractometry (XRPD) using a DRON-4-07 diffractometer (Cu Kα radiation; 40 kV, 20 mA). The structure parameters were refined by the Rietveld full profile analysis. XRPD patterns were collected in the range $2\Theta = 10–150°$ in step-scan mode with a step size of $\Delta 2\Theta = 0.02°$ and a counting time of 6 s per data point. As external standards, SiO_2 (for 2Θ) and Al_2O_3 NIST SRM1976 (for the intensity) were used. The temperature dependence of the electrical resistance of the samples was measured in the temperature range 20–400 °C. The microstructures of specimens were observed by field emission scanning electron microscopy REM 101 SEM (Sumy Electron Optics, Ukraine). Impedance data were obtained using a 1260 Impedance/Gain-phase Analyzer (Solartron Analytical) in the range 1–10^6 Hz The components of the equivalent circuit such as interior, boundary and outer layer region of grain were fitted to experimental data by using ZView software (Scribner Associates).

3. Results and discussion

The XRPD patterns of the powders calcined at temperatures lower than 1000 °C contain reflections of several phases. $BaTiO_3$ and $K_{0.5}Bi_{0.5}TiO_3$ were formed at 900 °C. The $(1-x)BaTiO_3–xK_{0.5}Bi_{0.5}TiO_3$ solid solutions were formed after heat treatment above 1000 °C in accordance with the scheme:

$$1-x\ BaTiO_3 + x\ K_{0.5}Bi_{0.5}TiO_3 = Ba_{1-x}K_{0.5x}Bi_{0.5x}TiO_3.$$

The parameters of the crystal structure of the ceramic samples were determined using Rietveld full-profile X-ray analysis (Fig. 1).

Table 1
Structure parameters of samples in $(1-x)BaTiO_3–xK_{0.5}Bi_{0.5}TiO_3$.

x	0.1	0.15	0.2
Unit cell parameters[a]			
a, Å	3.9909(8)	3.9861(8)	3.9824(2)
c, Å	4.0321(1)	4.0303(1)	4.0285(2)
V, Å^3	64.220(3)	64.037(3)	63.889(5)
Positions of ions (z/c)			
Ba/K/Bi	0.50(2)	0.482(5)	0.49(1)
O1	0.55(2)	0.51(1)	0.55(1)
O2	0.03(2)	0.070(7)	0.05(1)
Agreement factors			
R_B, %	6.46	7.29	8.18
R_f, %	5.11	6.07	8.81

[a] Space group *P4mm* (99), the positions of the ions are the following: Ba/K/Bi (1*b*) 1/2 1/2 *z*/*c*, Ti (1*a*) 0 0 0, O1 (1*a*) 0 0 *z*/*c*, O2 (2*c*) 1/2 0 *z*/*c*.

The effect of substitution of bismuth and potassium ions for barium ions on the structure parameters in $(1-x)BaTiO_3–xK_{0.5}Bi_{0.5}TiO_3$ is shown in Table 1. The a and c parameters and the unit cell volume decrease with increasing x. Decrease in unit cell volume with increasing x is due to large difference between the value of the ionic radius of bismuth (1.17 Å) and that of barium (1.42 Å) [9].

Fig. 2 shows the temperature dependence of the dielectric constant and the loss tangent of the $(1-x)BaTiO_3–xK_{0.5}Bi_{0.5}TiO_3$ solid solutions at 100 kHz. The temperature of maximum $\varepsilon(T)$, which corresponds to a phase transition, was observed to increase with x. Above the phase transition temperature, the dielectric permittivity of samples with $x = 0.1$ and 0.2 obeys the Curie–Weiss law. For sample with $x = 0.1$, the Curie–Weiss constant, C is 2.7×10^5 and Curie temperature, Θ is 138 °C, and for sample with $x = 0.2$, $C = 1.89 \times 10^5$ and $\Theta = 162$ °C. The permittivity peak

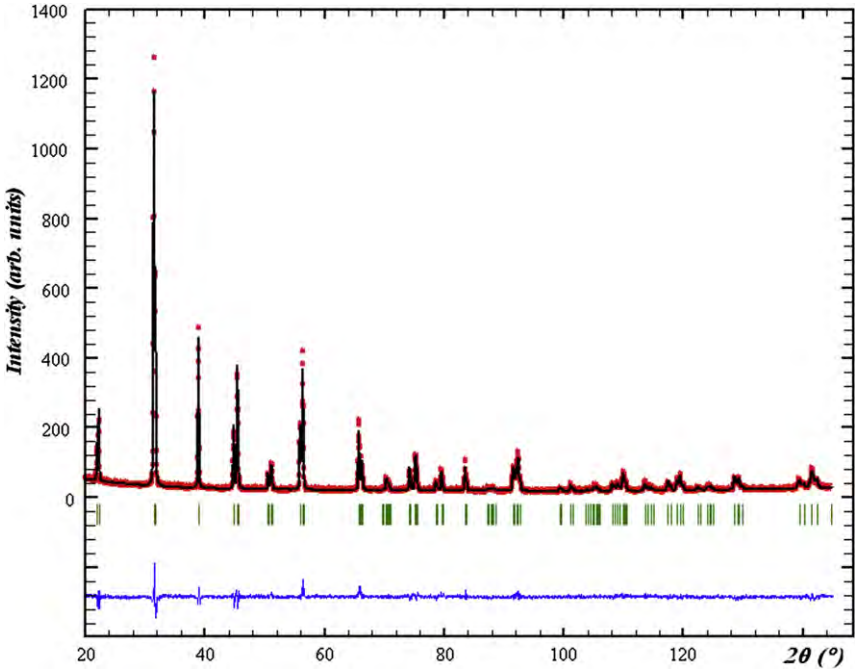

Fig. 1. Experimental (dots) and calculated (line) room-temperature powder X-ray powder diffraction patterns of $(1-x)BaTiO_3–xK_{0.5}Bi_{0.5}TiO_3$ solid solution: $x = 0.4$. Bars indicate the peak positions.

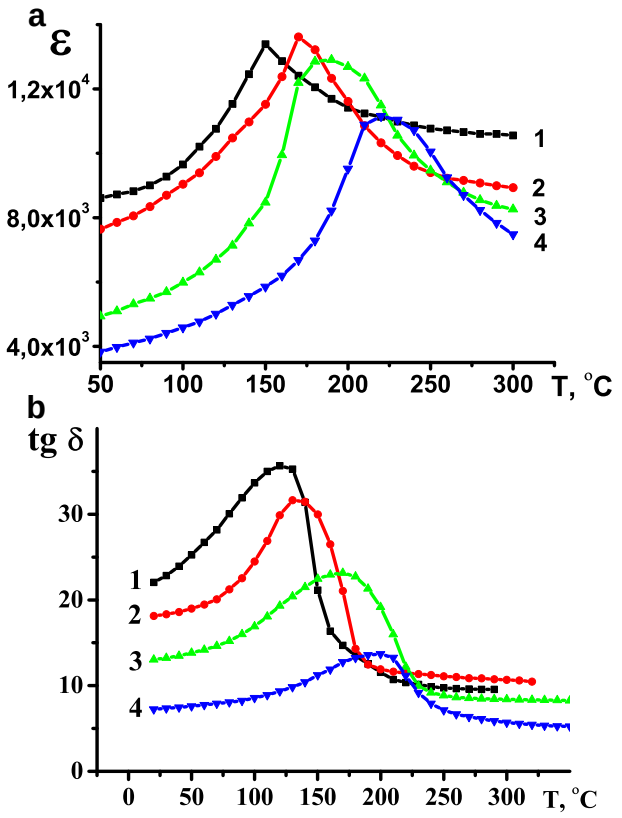

Fig. 2. Temperature dependence of the dielectric permittivity (a) and the loss tangent (b) of $(1-x)BaTiO_3$–$xK_{0.5}Bi_{0.5}TiO_3$ solid solutions, $x = 0.1$ (1), 0.2 (2), 0.3 (3), 0.4 (4). $f = 100$ kHz.

broadens in samples with $x = 0.3$ and 0.4. In this case, the temperature dependence of the permittivity ε near its maximum can be described by the equation [10]:

$$\varepsilon = \frac{\varepsilon_m}{1 + (T - T_m)^2/2\sigma} \quad (1)$$

where ε_m is maximum value of the dielectric permittivity; T_m is temperature corresponding to ε_m; σ is Gaussian blur coefficient. For sample with $x = 0.3$, ε_m is 13,024 and T_m is 196 °C and for sample with $x = 0.4$, $\varepsilon_m = 11{,}116$ and $T_m = 228$ °C.

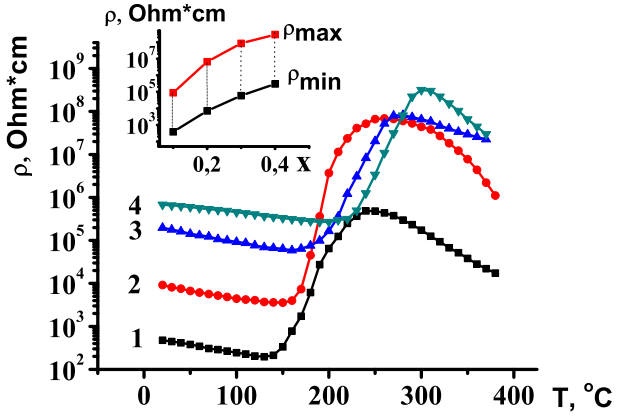

Fig. 3. Temperature dependence of resistivity of $(1-x)BaTiO_3$–$xK_{0.5}Bi_{0.5}TiO_3$ solid solutions, $x = 0.1$ (1), 0.2 (2), 0.3 (3), 0.4 (4). Inset: Plots of the maximum ρ_{max} and minimum ρ_{min} values of resistivity in $(1-x)BaTiO_3$–$xK_{0.5}Bi_{0.5}TiO_3$ solid solutions as a function of x.

Fig. 3 shows the temperature dependence of resistivity for $(1-x)BaTiO_3$–$xK_{0.5}Bi_{0.5}TiO_3$ solid solutions, where $x = 0.1$; 0.2 and 0.3. The ρ_{max}/ρ_{min} ratio decreases with increase in bismuth–potassium titanate concentration (see inset in Fig. 3). The values of ρ_{max} and ρ_{min} increase with increase in x (inset in Fig. 3). According to the results of calculations of α using formula $\alpha = (\ln(\rho_1/\rho_2)/dT)\cdot 100\%$ in system $(1-x)BaTiO_3$–$xK_{0.5}Bi_{0.5}TiO_3$, with $x = 0.1$; 0.2; 0.3, 0.4 α equals 8.2, 22, 11 and 10%/°C, respectively.

The grain size of sintered ceramics was found to decrease with increase in x (Fig. 4). This may be due to the segregation of K^+ ions

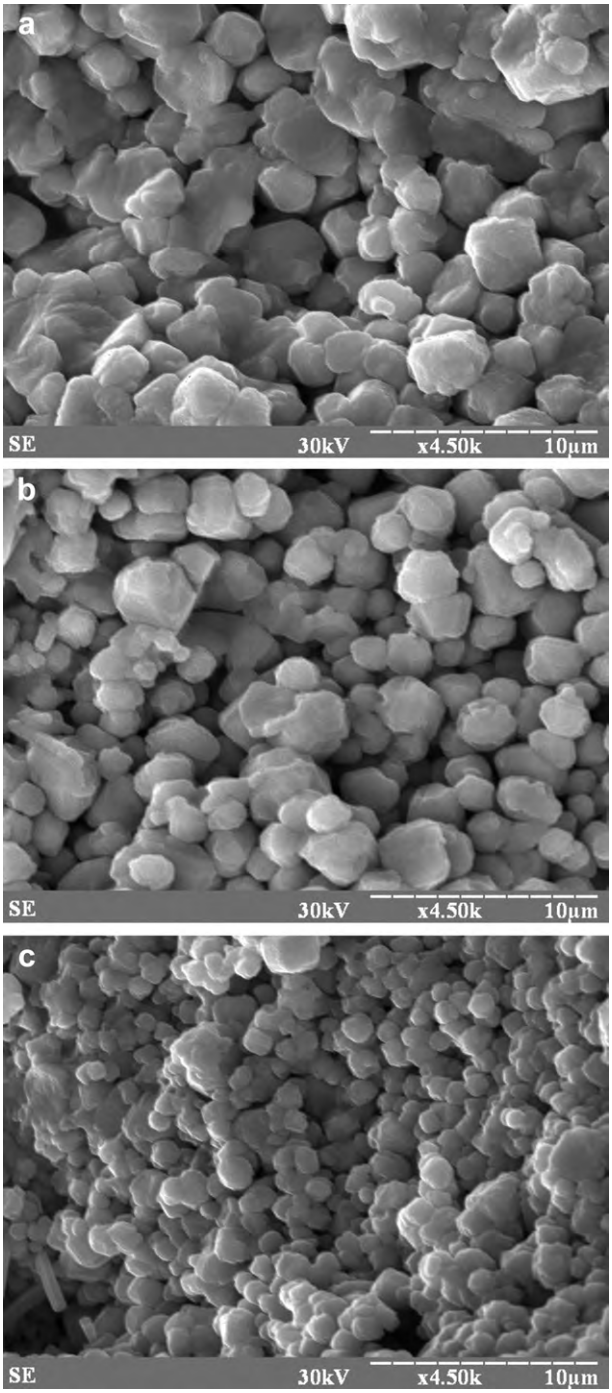

Fig. 4. Micrographs of $(1-x)BaTiO_3$–$xK_{0.5}Bi_{0.5}TiO_3$ solid solutions: (a) $x = 0.15$; (b) $x = 0.2$; (c) $x = 0.3$.

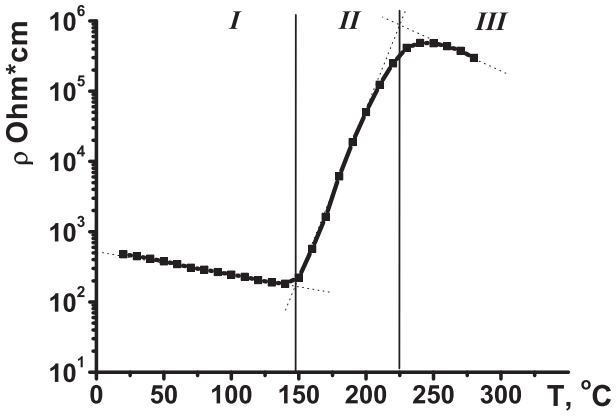

Fig. 5. Temperature dependence of resistivity for $Ba_{0.9}K_{0.05}Bi_{0.05}TiO_3$ solid solution.

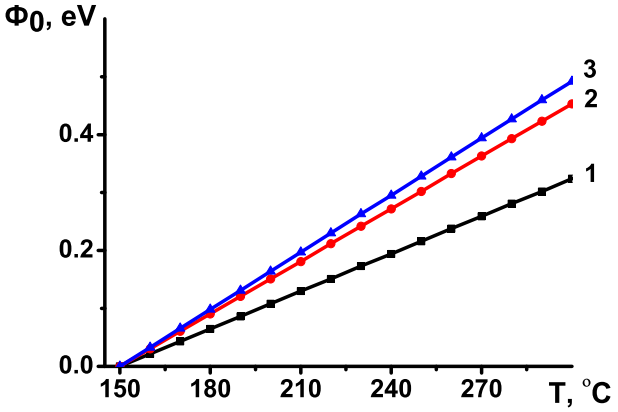

Fig. 6. Temperature dependence of the potential barrier for $(1-x)BaTiO_3$–$xK_{0.5}Bi_{0.5}TiO_3$ solid solutions, $x = 0.1$ (1), 0.2 (2), 0.3 (3).

near the grain boundaries and reduction of their mobility on densification. This retards the mass transport and, as a result, smaller grains are formed [11]. The grain size of ceramics in $(1-x)BaTiO_3$–$xK_{0.5}Bi_{0.5}TiO_3$ solid solutions decreases from 3.5 to 1 μm for $x = 0.1$ and 0.4 respectively.

As is known, the total number of insulating grain boundaries increases with decrease in the grain size of PTCR ceramics. This causes an increase in the total resistance of the material [12]. Therefore, the increase in the value of ρ_{min} and decrease in resistivity jump ρ_{max}/ρ_{min} with increase in x (inset in Fig. 3) for $(1-x)BaTiO_3$–$xK_{0.5}Bi_{0.5}TiO_3$ solid solutions may be attributed to a decrease in ceramic's grain size (Fig. 4).

The values of potential barriers at grain boundaries were calculated using the Heywang model [13]. In the regions I and II (Fig. 5), the variation of resistance with temperature is described by equations (2) and (3), respectively:

$$\rho_S = \rho_o \cdot e^{\frac{E_a^I}{kT}} \quad (2)$$

$$\rho = \alpha \cdot \rho_S \cdot e^{\frac{\Phi_0(T)}{kT}} \quad (3)$$

where ρ_o is a constant, E_a^I is the activation energy of conduction in the region I; k is Boltzmann constant, α is factor of the geometric configuration;

$\Phi_0(T)$ is the potential barrier height at grain boundaries:

$$\Phi_o(T) = \frac{e^2 \cdot n_D \cdot b^2}{2 \cdot \varepsilon_i(T) \cdot \varepsilon_o} \quad (4)$$

Here, e is the electronic charge (1.602×10^{-19} C), n_D is the bulk electron concentration, b is the barrier thickness ($2b = n_S = n_D$ where n_S – the surface density of acceptor states) and $\varepsilon_i(T)$ is the permittivity of the grain bulk. In ferroelectrics, ε_i obeys the Curie–Weiss law: $\varepsilon_i(T) = C/(T-\Theta)$ (C = Curie constant, Θ = Curie–Weiss parameter).

From equations (2) and (3) we obtain:

$$\rho = \alpha \cdot \rho_o \cdot e^{\frac{E_a^I}{kT}} \cdot e^{\frac{e^2 \cdot n_D \cdot b^2 (T-\Theta)}{2 \cdot \varepsilon_o \cdot C \cdot kT}} \quad (5)$$

Table 2
Parameters in Heywang model for $(1-x)BaTiO_3$–$xK_{0.5}Bi_{0.5}TiO_3$.

x	ρ_0, Ω cm	E_a^I, eV	$n_D \cdot b^2$, cm^{-1}
0.1	21	0.17	5.7×10^8
0.2	22	0.24	6.5×10^8
0.3	34	0.24	7.8×10^8

The results of calculations in accordance with equations (2)–(5) indicate that the activation energies in the region I increase with an increase in x (Table 2).

The changes in potential barrier with increase in x were calculated for region II using equation (4). The intergranular potential barrier height increases with increase in x (Fig. 6) which can be attributed to an increase in the number of acceptor states at the grain boundaries for example, due to the segregation of K^+ ions at grain boundaries, and this accounts for the behavior of ρ_{max} (Inset in Fig. 3) [14].

The results of investigations by the complex impedance method are presented as frequency dependences of the imaginary components of complex impedance Z'' and complex electric modulus M'' (Fig. 7). In accordance with [1,15], the shift of the peaks Z''_{max} and M''_{max} versus frequency is associated with a change in capacitance and resistance in the corresponding RC-circuit of equivalent circuit.

Fig. 7 shows that the peaks Z''_{max} and M''_{max} do not coincide in frequency. This indicates that the positions of the above maximums are determined by different regions of the ceramics. We interpreted the experimental results by using the model of PTCR for ceramic grains proposed by Sinclair and West [16,17]. According to this model, the grain in ceramics consists of several electrically heterogeneous regions, which can be represented by an equivalent circuit consisting of several parallel RC-elements connected in series. In particular, the change in the value and positions of the

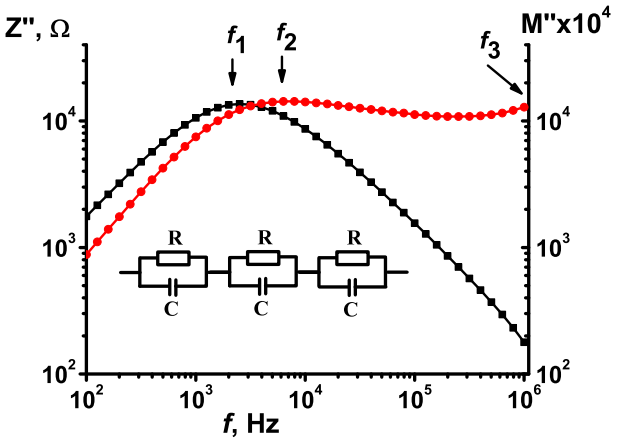

Fig. 7. Imaginary parts of complex impedance (Z'') and modulus (M'') for $Ba_{0.9}K_{0.05}Bi_{0.05}TiO_3$ solid solution. f_1, f_2 and f_3 relate to grain boundary, outer layer region and grain interior, respectively.

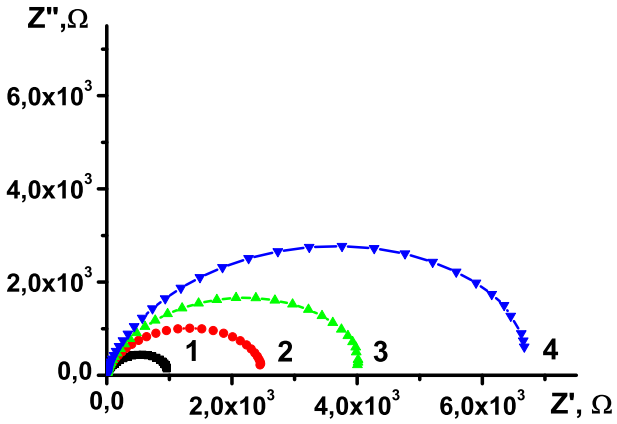

Fig. 8. Diagrams of complex impedance for $Ba_{0.9}K_{0.05}Bi_{0.05}TiO_3$ solid solution at 160 °C (1), 170 °C (2), 180 °C (3) and 190 °C (4).

maximums of $Z''(f)$ and $M''(f)$ are determined by the electrophysical properties of the following grain fractions: the grain boundaries determine the plot of $Z''(f)$, the grain outer layer is responsible for the plot of $M''(f)$ in the middle of the frequency range, whereas the grain interior determines the plot of $M''(f)$ at frequencies over 10^6 Hz.

The complex impedance results in the form of $Z'' = f(Z')$ plots at various temperatures are shown in Fig. 8. The value of real resistance Z' increases at temperatures above Curie temperature (Fig. 8), which is associated with an increase in potential barrier at the grain boundaries (Fig. 6).

The resistances of different regions of grain were calculated using the plot $Z'' = f(Z')$ (Fig. 8). Fig. 9 shows that the grain interior resistance varies a little in the investigated temperature range (Fig. 9, curve 1). At the same time the resistances of the outer layer region and the grain boundary increase sharply in the temperature range above the Curie temperature (Fig. 9, curves 2 and 3). This indicates that the outer layer region and the grain boundary make a contribution to the PTCR effect in $(1-x)BaTiO_3$–$xK_{0.5}Bi_{0.5}TiO_3$ solid solutions.

With increasing x the resistances of grain boundary and outer layer region were observed to increase (Fig. 10). The ratio of the maximum grain boundary resistance (Rb) to the maximum outer layer region resistance (Ro) increases with increasing x (inset in Fig. 10). A significant increase in the maximum resistance of the grain boundary may be associated with an increase in the total

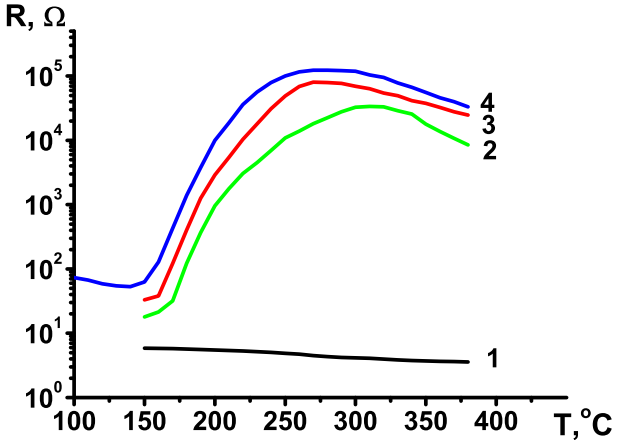

Fig. 9. Resistance of the grain interior (1), outer layer (2), grain boundary (3) and overall resistance (4) for $Ba_{0.9}K_{0.05}Bi_{0.05}TiO_3$ solid solution.

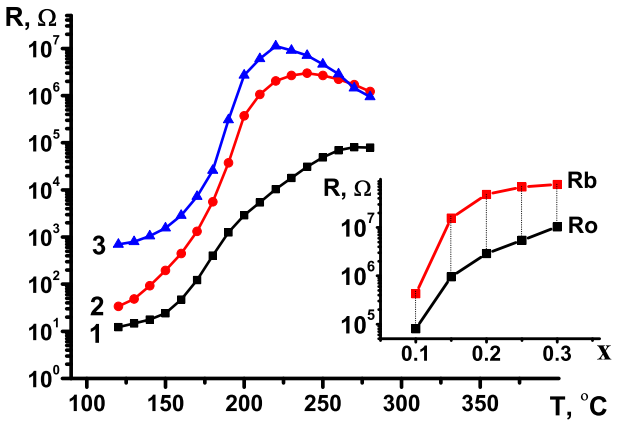

Fig. 10. Temperature dependence of grain boundaries resistance for solid solutions $(1-x)BaTiO_3$–$xK_{0.5}Bi_{0.5}TiO_3$, $x = 0.1$ (1), 0.2 (2), 0.3 (3). Insert: Plots of the maximum values of grain boundary and outer layer region resistances in $(1-x)BaTiO_3$–$xK_{0.5}$-$Bi_{0.5}TiO_3$ solid solutions as a function of x.

number of grain boundaries and the potential barrier at grain boundaries.

4. Conclusions

Solid solutions of $(1-x)BaTiO_3$–$xK_{0.5}Bi_{0.5}TiO_3$ were prepared by the solid state reaction technique. Sintering of samples was carried out in reducing atmosphere of N_2/H_2 in the temperature range 1100–1240 °C with subsequent oxidation at 700 °C. The crystal structure of solid solutions was confirmed by XRPD. With increasing x the grain size decreases. The resistivity jump ρ_{max}/ρ_{min} decreases with increase in x. At the same time, the value of ρ_{min} increases, which may be attributed to an increase in the number of insulating grain boundaries due to a decrease in the grain size of the ceramics. With increasing x the Curie temperature of solid solutions $(1-x)BaTiO_3$–$xK_{0.5}Bi_{0.5}TiO_3$ ($0 \le x < 0.4$) increases from 150 to 220 °C. Using the Heywang model it was shown that the value of the potential barriers at the grain boundaries increases with increasing x. The complex impedance results indicate that there are three areas of grain with different electrical properties in the system $(1-x)BaTiO_3$–$xK_{0.5}Bi_{0.5}TiO_3$. The outer layer region and the grain boundary were found to make a contribution to the PTCR effect in $(1-x)BaTiO_3$–$xK_{0.5}Bi_{0.5}TiO_3$ solid solutions.

References

[1] F.D. Morrison, D.C. Sinclair, A.R. West, Characterization of lanthanum-doped barium titanate ceramics using impedance spectroscopy, J. Am. Ceram. Soc. 84 (2001) 531–538.
[2] P. Bomlai, N. Sirikulrat, A. Brown, S.J. Milne, Effects of TiO_2 and SiO_2 additions on phase formation, microstructures and PTCR characteristics of Sb-doped barium strontium titanate ceramics, J. Eur. Ceram. Soc. 25 (2005) 1905–1918.
[3] O.Z. Yanchevskii, O.I. V'yunov, A.G. Belous, Fabrication and properties of semiconducting barium lead titanate ceramics containing low-melting glass additions, Inorg. Mater. 39 (2003) 645–651.
[4] Directive 2002/95/Ec of the European parliament and of the council of 27 January 2003 on the restriction of the use of certain hazardous substances in electrical and electronic equipment, Off. J. Eur. Union L 37 (2003) 19–23.
[5] E.I. Bondarenko, A.N. Pavlov, I.P. Raevskii, I.P. Prokopalo, Positive temperature coefficient of resistivity in potassium-bismuth titanate, Solid State Phys. 27 (1985) 2530–2533.
[6] P.H. Xiang, H. Harinaka, H. Takeda, T. Nishida, K. Uchiyama, T. Shiosaki, Annealing effects on the characteristics of high T_c lead-free barium titanate-based positive temperature coefficient of resistivity ceramics, J. Appl. Phys. 104 (2008) 094108.
[7] H. Takeda, H. Harinaka, T. Shiosaki, M.A. Zubair, C. Leach, R. Freer, T. Hoshina, T. Tsurumi, Fabrication and positive temperature coefficient of resistivity properties of semiconducting ceramics based on the $BaTiO_3$–$(Bi_{1/2}K_{1/2})TiO_3$ system, J. Eur. Ceram. Soc. 30 (2010) 555–559.

[8] S. Leng, G. Li, L. Zheng, T. Wang, Q. Yin, Synthesis of Y-doped $BaTiO_3$–$(Bi_{1/2}K_{1/2})TiO_3$ lead-free positive temperature coefficient of resistivity ceramics and their PTC effects, J. Am. Ceram. Soc. 92 (2009) 2772–2775.
[9] R.D. Shannon, Revised effective ionic radii and systematic studies of interatomic distances in halides and chalcogenides, Acta Crystallogr. A32 (1976) 751–767.
[10] S.A. Gridnev, A.A. Kamynin, Specific features of the polarization in the $PbFe_{1/2}Nb_{1/2}O_3$ ferroelectric, Phys. Solid State 54 (2012) 1018–1020.
[11] C. Zhou, X. Liu, W. Li, C. Yuan, Structure and piezoelectric properties of $Bi_{0.5}Na_{0.5}TiO_3$–$Bi_{0.5}K_{0.5}TiO_3$–$BiFeO_3$ lead-free piezoelectric ceramics, Mater. Chem. Phys. 114 (2009) 832–836.
[12] D.Y. Wang, K. Umeya, Electrical properties of PTCR barium titanate, J. Am. Ceram. Soc. 73 (1990) 669–677.
[13] W. Heywang, Semiconducting barium titanate, J. Mater. Sci. 6 (1971) 1214–1226.
[14] O.I. V'yunov, L.L. Kovalenko, A.G. Belous, V.N. Belyakov, Distribution of manganese ions and its effect on the properties of PTCR ceramic, Inorg. Mater. 39 (2003) 190–197.
[15] F.D. Morrison, D.C. Sinclair, A.R. West, Anomaly in La-doped $BaTiO_3$, J. Am. Ceram. Soc. 84 (2001) 474–476.
[16] D.C. Sinclair, A.R. West, Use of succinic acid to test the stability of PTCR barium titanate ceramics under reducing conditions, J. Am. Ceram. Soc. 78 (1995) 241–244.
[17] A.R. West, D.C. Sinclair, N. Hirose, Characterization of electrical materials, especially ferroelectrics, by impedance spectroscopy, J. Electroceram. 1 (1997) 65–71.